Fatigue life assessment in lateral support element of a magnet for nuclear fusion experiment "Wendelstein 7-X"

V. Giannella[a], J. Fellinger[b], M. Perrella[a] and R. Citarella[a]

[a] Department. of Industrial Engineering, University of Salerno, via Giovanni Paolo II 132, Fisciano (SA), Italy,

[b] Max-Planck-Institut Für Plasmaphysik, Teilinstitut Greifswald, Greifswald, Germany

Abstract

Wendelstein 7-X (W7X), a nuclear fusion experiment of modular stellarator type, started operation in 2015 and will be upgraded with a water cooled first wall for steady state operation in 2020. A hot hydrogen plasma of ultra-low density is confined in a plasma vessel by an electromagnetic field generated by specially shaped superconducting coils. Such coils, embedded in a cryostat working at 4K, are kept by a central support ring and joined together by welded lateral support elements (LSEs). In this paper, a FEM-DBEM (Dual BEM) submodelling approach is adopted for crack-growth simulations of the cracks detected in LSEs and driven by fatigue load spectra.
A global analysis on one fifth of the fivefold symmetric magnet system is performed by FEM, whereas, the submodelling approach is adopted to solve the crack propagation by DBEM. In particular, the adopted approach is based on the application of the superposition principle to solve a LEFM problem: the only boundary conditions for the DBEM submodel consist of tractions, calculated by the FEM global analysis and applied to the crack faces in the local submodel. The obtained speed of crack advance and crack kinking are compared with literature results to highlight the accuracy of the propose approach together with inherent computational advantages.

Keywords: Wendelstein 7-X, superposition principle, FEM-DBEM, crack propagation, load spectrum

Nomenclature

C = Paris' law coefficient
C' = Forman's law coefficient
E = Young's modulus
J = J-integral
K = Stress Intensity Factor
R = loading ratio
T = Tension vector on crack faces
W = strain energy density
da/dN = crack propagation rate
m = Paris' law exponent
n = Forman's law exponent
s = abscissa along crack path
u = displacement component in direction along crack faces
ΔK = Stress Intensity Factor range
K_c = critical value of Stress Intensity Factors
K_{eff} = effective value of Stress Intensity Factors
ΔK_{th} = threshold value of Stress Intensity Factor range
Γ = closed path around crack tip
α = thermal expansion coefficient

ν = Poisson's ratio

1. Introduction

The world's largest nuclear fusion experiment of stellarator type Wendelstein 7-X (W7-X) is currently in operation at the Max-Planck-Institute for Plasma Physics in Greifswald, Germany (Fig. 1a) [1]. The hot hydrogen plasma is confined in a Plasma Vessel (PV) by an electromagnetic (EM) field (Fig. 1b), with a magnitude up to 3 T, provided by 50 non-planar and 20 planar superconducting coils (Fig. 1c). Measurements of the magnetic field under operating conditions confirmed the accuracy and rigidity of the magnet system [2].
In the vacuum created inside the cryostat, the coils are cooled down to a superconducting temperature, close to absolute zero (4 K), using helium liquid. The magnetic cage, keeps the 30 cubic metres of ultra-thin plasma suspended inside the plasma vessel. Such plasma is heated up to fusion temperature by microwave heating, allowing for the separation of the electrons from the nuclei of the helium or hydrogen atoms.
During the initial operations, helium and subsequently hydrogen plasma were continuously produced in W7-X with pulse lengths varying from half a second to six seconds and temperatures up to 100 million degrees Celsius [3].
Coils are bolted onto a central supporting structure and interconnected by welded Lateral Support Elements (Fig. 1d): 100–150 mm long hollow tubes of 30–35 mm thickness made of forged stainless steel EN 1.4429.

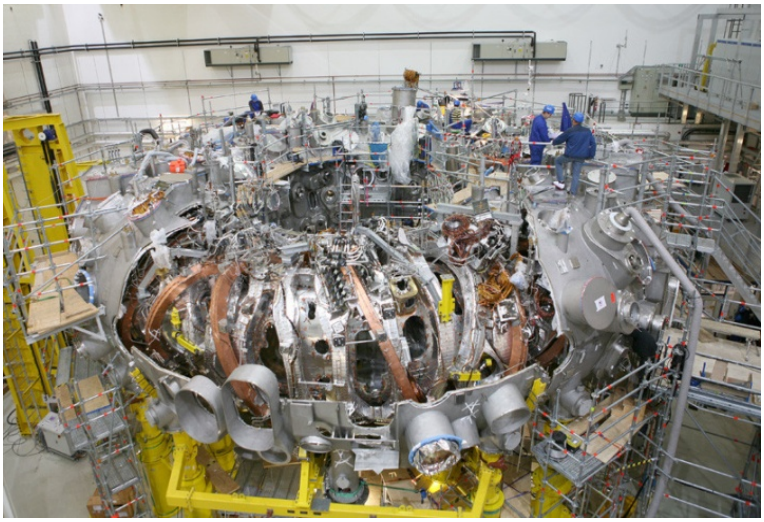

Figure 1. (a) Modular-type stellarator Wendelstein 7-X.

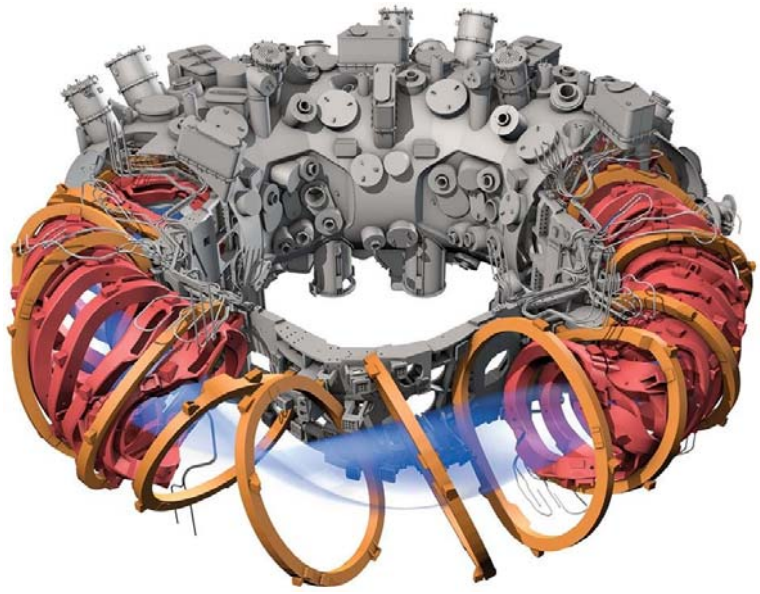

Figure 1. (b) Hot plasma confined by EM field generated by the coils.

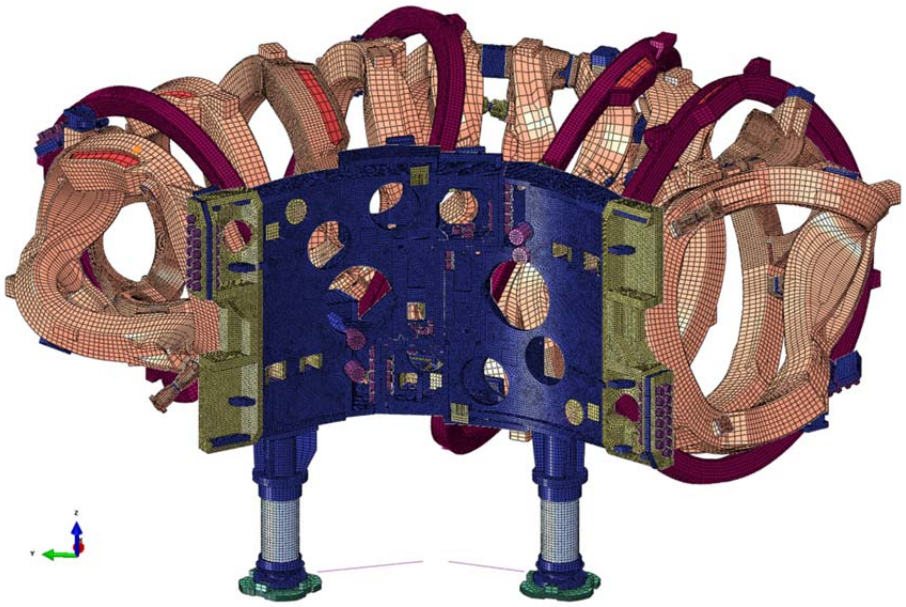

Figure 1. (c) FEM assembly of one-fifth of the magnet system of W7-X.

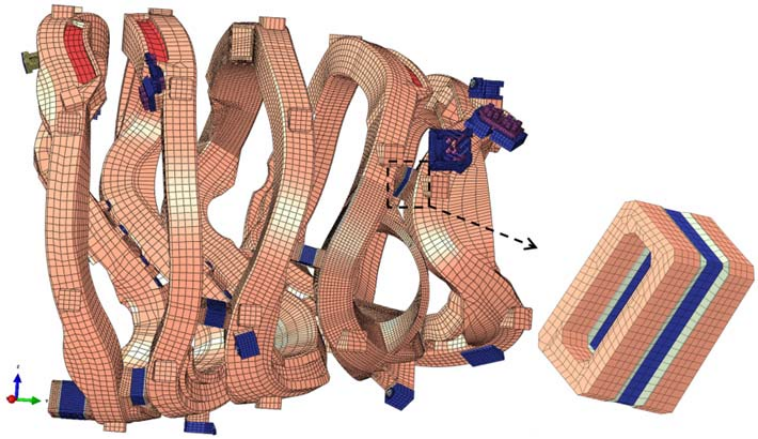

Figure 1. (d) Magnet system of W7-X: FEM detail of a half module with the LSEs; highlights on the investigated LSE-05.

After the welding of the LSEs to the coil cases (weld depth 15-30 mm), several surface cracks larger than 8 mm (typical acceptance limit of EN 23277 [4]) were found near the welds that could potentially limit the W7-X operations. Cracks were found with visual inspection and dye penetration tests at the accessible surfaces, particularly at the coil side of the weld within the cast steel, oriented mainly parallel to the weld seam (Fig. 2). Such cracks, in coils and superconducting cables areas where high stresses develop [5], can become critical during operations.

In order to take advantage of the high accuracy and flexibility of DBEM [6-9] when handling 3D crack-growths under mixed-mode conditions, in [10] such cracks were modelled using a coupled FEM-DBEM approach [11-13]. Crack sizes as well as stress-state and SIFs along the crack front were step-by-step updated through the entire simulation, and the crack-growth was continued until the critical SIF was reached. The crack depth was not pointed out by NDI (Non-Destructive Inspection) tests; however from repair experience it was found that such size is typically smaller than half the superficial crack length.

In [14], the same problem was tackled considering the simultaneous propagation of multiple cracks up to a condition of coalescence.

In this work, the most critical discovered crack (Fig. 2) was modelled, as done in [14], but with a different FEM-DBEM approach, leveraging on the superposition principle to gain computational advantages. In particular, as stated by the superposition principle applied to LEFM problems [15], SIFs can be calculated by means of a submodel analysis in which the boundary conditions, in terms of tractions, are applied only on the crack faces. The complex global analysis of one fifth of the whole fivefold W7-X magnet system is still

demanded to the FEM approach, whereas, the fracture problem is worked out by means of a DBEM model, whose boundary conditions are derived from the FE stresses calculated analysing the uncracked global domain. The advantages of using such Loaded Crack (LC) approach, whose theoretical background is well described in [11], are here presented and the results are compared with those obtained in [14].
In particular, the approach adopted in [10] computes the whole crack-growth by assuming "fixed displacement" boundary conditions (hereinafter "FD"), with the resultant life-prediction that turns out to be non-conservative. Another option would be to apply traction boundary conditions on the submodel cut surfaces and consider them invariable ("fixed load" condition, hereinafter "FL") for the whole crack growth phase, with the resultant life-prediction that turns out to be on the safe side.
Differently from the two previously mentioned approaches, the results presented in this paper are computed by updating step-by-step a traction distribution on the elements of crack faces: once SIFs are computed by DBEM and the extended crack is inserted into the model, new tractions are applied on the added elements, by resorting to the FEM stresses previously computed, in the same position, solving the stress problem for an uncracked domain.
The SIF values corresponding to the initial crack configuration are expected to be equal to those obtained when using FD or FL assumptions, whereas differences will start to emerge during the propagation, because, differently from the two aforementioned approaches, using LC approach the boundary conditions are continuously updated along the propagation. Moreover, the LC life-prediction is expected to be in between the predictions computed by FD and FL approaches.
ABAQUS [16] and BEASY [17] commercial codes are adopted for FEM and DBEM analyses respectively.

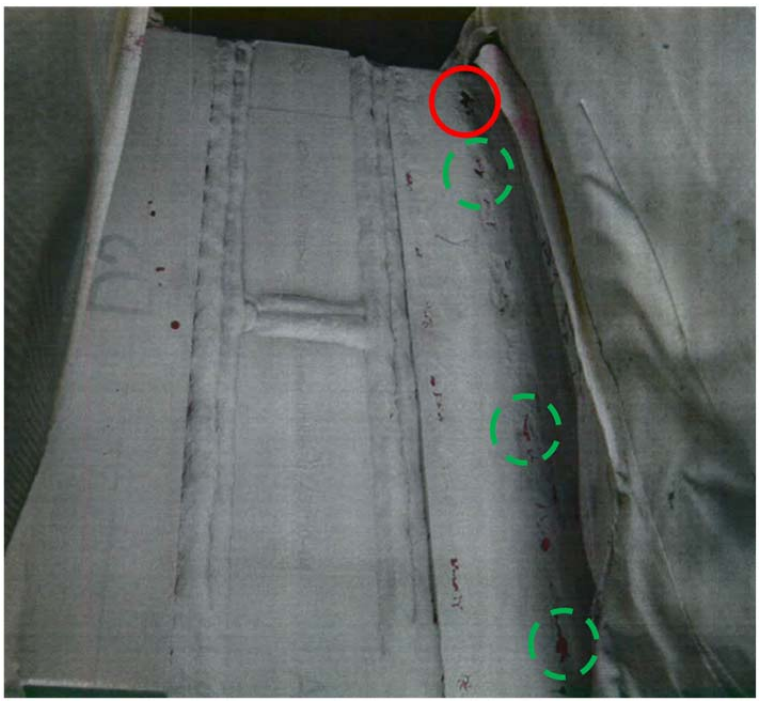

Figure 2. LSE-05: real component with highlight of discovered surface cracks; continuous circle (red line) surrounding the most critical (and modelled) crack.

2. FEM modelling

A global FEM model of one fifth of the five-fold symmetric W7-X magnetic cage has been developed (Fig. 3a) considering, in addition to the magnetic loads: bolt preloading, dead weight and cooling. Then, a FEM submodelling analysis (Fig. 3b) in the zone around the most critical crack (Fig. 2) has been made, without any crack introduction. A further FEM submodelling has been produced (Fig. 3c) in order to get a more accurate stress assessment on the investigated area. Such stress field must be computed with the highest accuracy because it will provide the input for the subsequent DBEM fracture assessment.

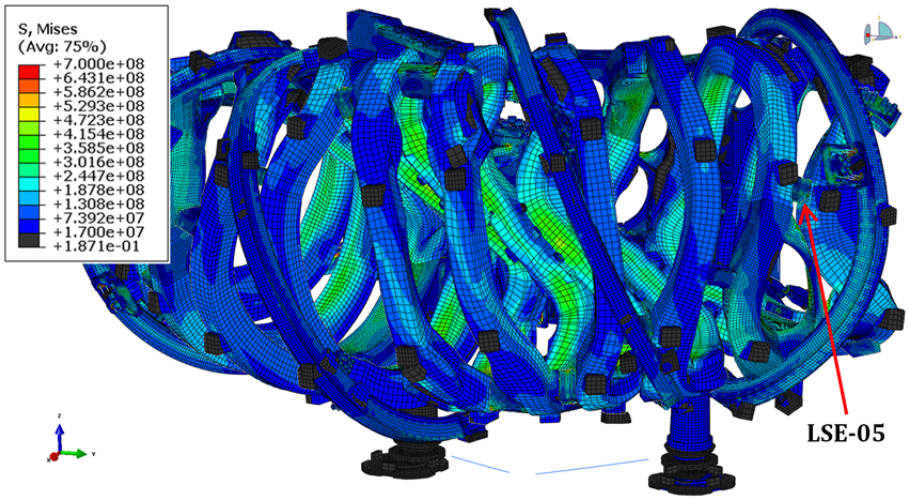

Figure 3. (a) von Mises stresses (Pa) on FEM global model; red arrow pointing out the analysed LSE-05; load case with EM field of 3T "HJ".

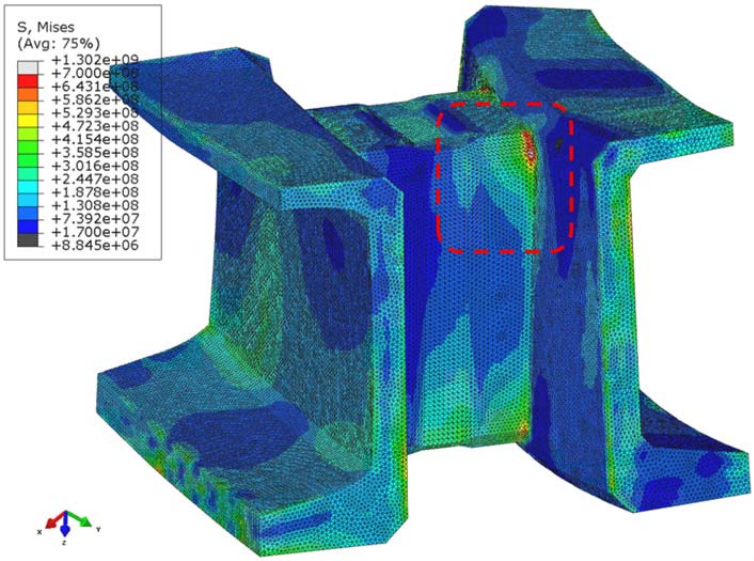

Figure 3. (b) von Mises stresses (Pa) on FEM submodel of LSE-05; dashed red square representing the area that will be furtherly refined; load case with EM field of 3T "HJ".

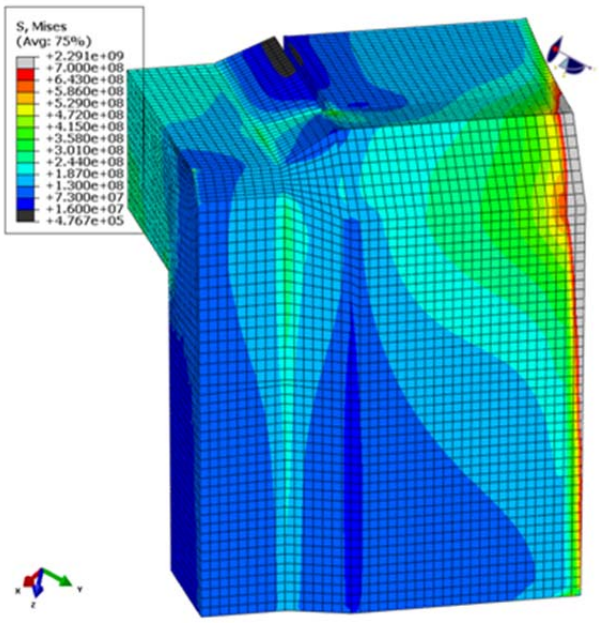

Figure 3. (c) von Mises stresses (Pa) on the furtherly refined FEM submodel; load case with EM field of 3T "HJ".

3. DBEM modelling

The DBEM modelling is aimed at simulating the propagation of a semi-circular crack. For this purpose, the crack growth simulations are performed by using a DBEM cracked submodel, with crack faces loaded by tractions extracted by the solution of an uncracked FEM submodel.
The crack path is assessed by resorting to the Minimum Strain Energy Density criterion [18] and the Stress Intensity Factors (SIFs) along the crack front are calculated by the *J*-integral approach [19, 20].
An un-cracked BEM model (Fig. 4b) is extracted from the aforementioned FEM submodel (Fig. 4a), by a Boolean operation of subtraction of a spherical domain, centred on the most critical crack. Then, a semi-circular crack with radius equal to 7 mm is inserted (Fig. 5), switching from a BEM to a DBEM formulation, in order to analytically tackle the singularity introduced by the crack modelling.
The spherical domain must be sized in such a way to have a sufficiently high distance between crack boundaries and cutting surfaces, in such a way to allow a complete stress state dying out, from the crack surroundings to the subdomain boundaries (as dictated by the applied superposition procedure).
A preliminary convergence study was aimed at evaluating such minimum DBEM model size and the results of such optimal model are here presented. In particular, the optimal spherical cut has a radius equal to 0.11 m.
The adopted material properties are listed in Table 1 (see Fig. 5 for zone definition).

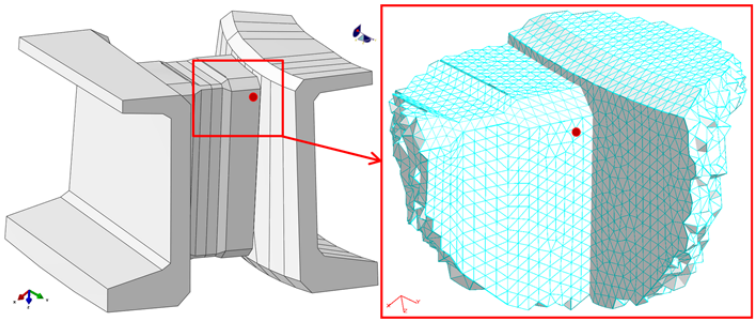

(a) (b)

Figure 4. (a) FEM submodel and (b) DBEM uncracked submodel (the red dot is the crack insertion point), obtained by a Boolean subtraction with a sphere of radius 0.11 m.

	E (GPa)	υ (-)	α (μm/(mK))
Zone 1 EN 1.4429	197	0.3	10.38
Zones 2, 3 EN 1.3960	158	0.3	10.2

Table 1. Mechanical properties at 4K temperature.

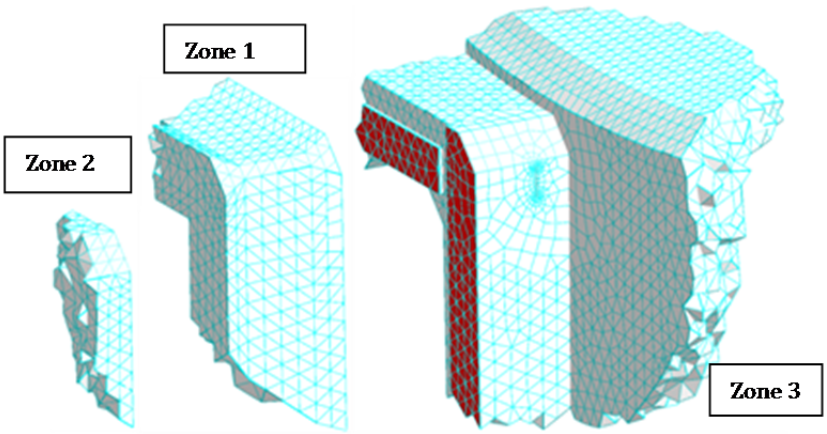

Figure 5. DBEM cracked submodel with highlight of the different modelled zones.

The initial DBEM mesh includes nearly 5300 elements: the crack faces as well as the crack surroundings are remeshed step-by-step by using fully quadratic elements whereas the non remeshed areas keeps linear elements. At the last considered propagation step, in correspondence of the biggest crack sizes, the number of elements rises up to nearly 5800.

4. Superposition principle applied to LEFM

The LC approach can be described assuming, for example, the thermal-stress problem schematically shown in Figs. 6-7, where the general crack problem can be divided in two steps:

- starting from an uncracked domain (*a*), a crack can be opened (*b*) and loaded with tractions equal to those calculated over the dashed line of the virtual crack in (*a*);
- the new configuration (*b*), perfectly equivalent to the previous one (*a*), can be solved by using the superposition principle, splitting the boundary conditions as in (*c*) and (*d*): (*c*) represents the fracture problem we are interested to solve, whereas (*d*), after the sign inversion of the tractions on the crack faces (*e*), represents an alternative equivalent problem that is possible to solve instead of the more complex problem (*c*).

Using boundary conditions coming from the considered thermal-stress uncracked problem, a pure stress crack problem (*e*) can be solved, in which crack faces are subjected to tractions equal in magnitude but opposite in sign to those calculated over the dashed line in (*a*). This is possible as SIFs for case (*c*) are equal (Eqs. 1, 2) to those calculated for case (*e*) shown in Fig. 7.

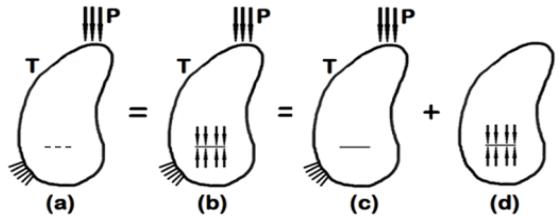

Figure 6. Superposition principle applied to LEFM problems.

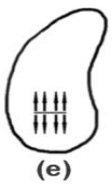

Figure 7. Solved problem by DBEM analysis.

$$K_a = K_b = 0 = K_c + K_d \qquad (1)$$

$$K_c = -K_d = K_e \qquad (2)$$

Different alternatives of boundary conditions can be taken into account when working out the LEFM problem (Fig. 8). Fig. 8b represents the DBEM model with LC approach: load boundary conditions are only applied on the crack faces and continuously updated along the crack extension. Alternatively, Fig. 8a and Fig. 8c show boundary conditions applied on the DBEM cut surfaces, in terms of displacements or tractions respectively: in this case the crack-growth is solved under an FD or FL assumption with no update of BCs during propagation. Furthermore, the BCs for FD or FL are typically computed by resorting to a FEM model that does not contain a crack, with an inherent approximation whose impact on the solution accuracy can be restricted only resorting to a large enough DBEM submodel, in such a way to keep the cut surfaces sufficiently far from crack boundaries. On the other hand, enlarging the submodel will affect the computational burden.

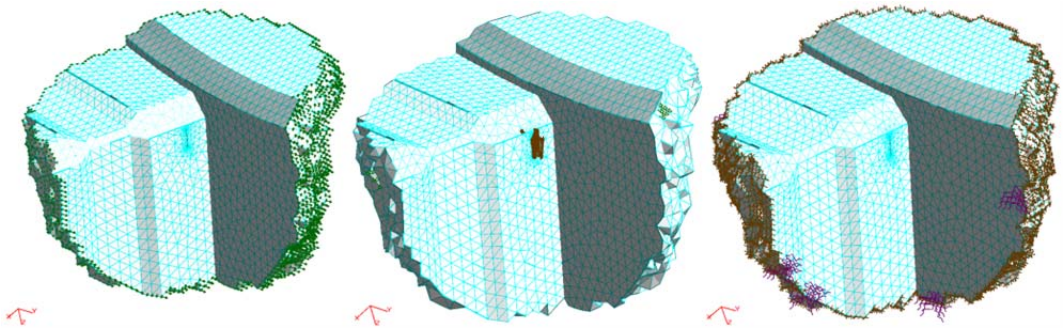

(a) (b) (c)

Figure 8. DBEM submodel loaded with different BCs: either displacements (a) or tractions (c) applied on cut surfaces; tractions applied on the crack faces (b).

When using the LC approach, an uncracked FEM model is necessary to accurately compute the stress field in the surroundings of the cracked zone, whereas, the fracture problem is completely demanded to the DBEM analysis. All the loads applied to the real component (viz. thermal, electro-magnetic, dead weight, bolt preloading) are incorporated by the FEM analysis, whereas, the SIFs evaluation and subsequently the whole crack-growth is worked out into the DBEM environment by means of a step-by-step pure stress analyses.
A further advantage of such LC approach is given by the possibility to study crack propagation with a significantly smaller model than needed by FD or FL approaches, as enabled by the self-equilibrated nature of the load applied with LC and its rapidly vanishing effects when getting far apart from the crack.
Such Reduction of the DBEM model size will strongly speed up the calculations.

5. Load Spectra

The load spectra, corresponding to the sequence of five load changes on the magnet, are applied to the DBEM submodel through different boundary condition sets. Such boundary condition sets are obtained from five different FEM global analyses and corresponding FEM submodel analyses. A qualitative visual description of the loading history due to the Lorentz forces is provided in Fig. 9.

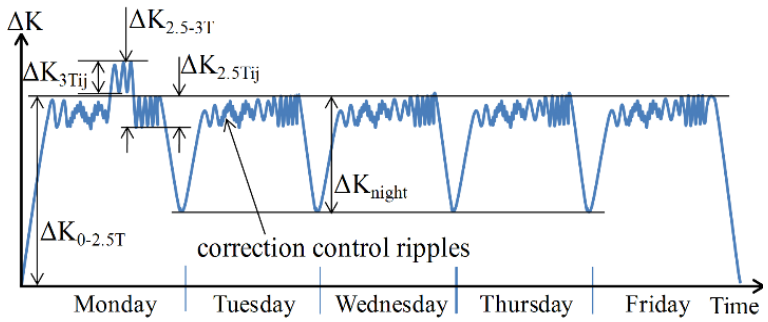

Figure 9. Schematic loading history due to EM forces.

The FEM analyses are performed using different electromagnetic loadings, then creating the following five load cases:

i. magnetic field with magnitude equal to 2.5 T with a given orientation (termed "HJ");
ii. magnetic field with magnitude equal to 2.5 T with a different orientation (termed "LS");
iii. magnetic field with magnitude equal to 3 T in "HJ" configuration;
iv. magnetic field with magnitude equal to 3 T in "LS" configuration;
v. magnetic field with magnitude equal to 1.7 T in "HJ" configuration. This load corresponds to the reduced magnetic field at night.

The DBEM crack faces will undergo the five aforementioned loading conditions, applied in predefined sequences simulating two different load spectra:

— daily spectrum, using only the load steps from *i* to *iv*; load step *v* is excluded. In this load spectrum, it is assumed that the magnets are turned off at night; the sequence showed in Table 2 is repeated up to a condition of crack instability;
— weekly spectrum, useing all of the five load cases *i* to *v*; the sequence showed in Table 3 is repeated up to a condition of crack instability.

The plan is that the magnet system will remain loaded for a 5-days week of experimental operations, with or without a limited reduction of the electromagnetic (EM) field at nights (Fig. 9).

Cycles in each block	EM field (minimum magnitude)	EM field (maximum magnitude)
10	0	2.5 T ("HJ" config.)
100	2.5 T ("LS" config.)	2.5 T ("HJ" config.)
1	0	3 T ("HJ" config.)
10	3 T ("LS" config.)	3 T ("HJ" config.)

Table 2. Fatigue elementary block corresponding to 10 working days with the daily spectrum (12.1 cycles per working day).

Cycles in each block	EM field (minimum magnitude)	EM field (maximum magnitude)
10	0	2.5 T ("HJ" config.)
200	2.5 T ("LS" config.)	2.5 T ("HJ" config.)
1	0	3 T ("HJ" config.)
20	3 T ("LS" config.)	3 T ("HJ" config.)
40	1.7 T ("HJ" config.)	2.5 T ("HJ" config.)

Table 3. Fatigue elementary block corresponding to 50 working days with the weekly spectrum (5.42 cycles per working day).

During an experimental campaign, the EM field can be shifted several times from one configuration to another (HJ to LS and vice versa) with changes involving the EM field direction; moreover there can be also changes to the EM field magnitude, from 2.5 T to 3 T and vice versa.
Consequently, in order to estimate the operation limits, the following SIF increments are considered: $\Delta K_{0\text{-}2.5T}$ due to start-up of the machine on monday morning from 0 to 2.5 T; $\Delta K_{2.5\text{-}3T}$ due to increase from 2.5 T to 3 T; $\Delta K_{2.5Tij}$ and ΔK_{3Tij}, each one due to shift from one EM configuration to another and 2.5 T to 3 T respectively; in case of weekly spectrum, ΔK_{night} is added. Changes in the EM field for plasma ripple control are considered as small enough to be neglected.
The crack-growth for the load cycles from 0-2.5 T is predicted using the Paris' law [21]:

$$\frac{da}{dN} = C\Delta K^m \quad (3),$$

with the related material parameters listed in Table 4, as derived from FCGR test series carried out at cryogenic temperatures.
The crack-growth-rate (CGR) for the other cycles (in which stress ratio $R \neq 0$) is predicted using a Forman's law [22]:

$$\frac{da}{dN} = \frac{C'(\Delta K)^n}{(1-R)K_c - \Delta K} \quad (4),$$

with the related parameters listed in Table 5.
C values are consistent with ΔK units [Pa*m$^{0.5}$] and *da* units [mm].

	Zone 3 - EN 1.3960
C [-]	3.314 E-32
m [-]	3.23
ΔK_{th} [Pa√m]	15
ΔK_c [Pa√m]	1.6 E8

Table 4 Paris' law parameters at 4K temperature

	Zone 3 - EN 1.3960
C' [-]	1.162 E-17
n [-]	2.36
ΔK_{th} [Pa√m]	15
ΔK_c [Pa√m]	1.6 E8

Table 5 Forman's law parameters at 4K temperature

6. Results

Weekly load spectrum

The DBEM model is loaded with the results evaluated by FEM submodel analyses for the five different magnetic configurations corresponding to the weekly load spectrum. In doing this, the DBEM model has been loaded applying five sets of traction boundary conditions just on the crack faces (Fig. 10), by resorting to the FEM stress fields evaluated along the virtual path of the crack. A first attempt of using stresses coming from the FEM submodel shown in Fig. 3b did not produce accurate results, so it was necessary to further refine the mesh in the crack surroundings (Fig. 3c). This is expected because the accuracy of DBEM results (SIF values) is completely dependent on the accuracy of stress evaluations on the virtual crack faces provided by the FEM submodel solution.
Because of such peculiar DBEM boundary conditions, the DBEM stress field is not representative of the real stress scenario throughout the whole component but is anyway useful to determine accurately SIFs along the crack front.
The DBEM stress fields computed by the Loaded Crack (LC) and Fixed Displacement (FD) (the latter, when considering the initial crack configuration, is equal to that produced under FL conditions) are reported in Figs. 11-12 respectively. Such results are related to the initial crack configuration and the most critical load case N° 3, with an EM field applied with magnitude 3 T in configuration "HJ".

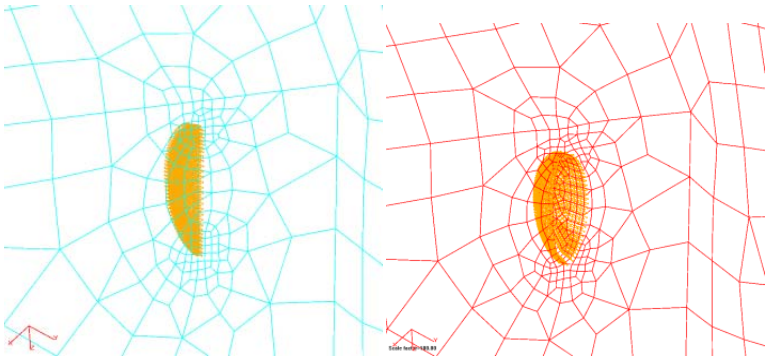

(a) (b)

Figure 10. (a) Initial DBEM crack shape (tractions in orange); corresponding deformed shape (b).

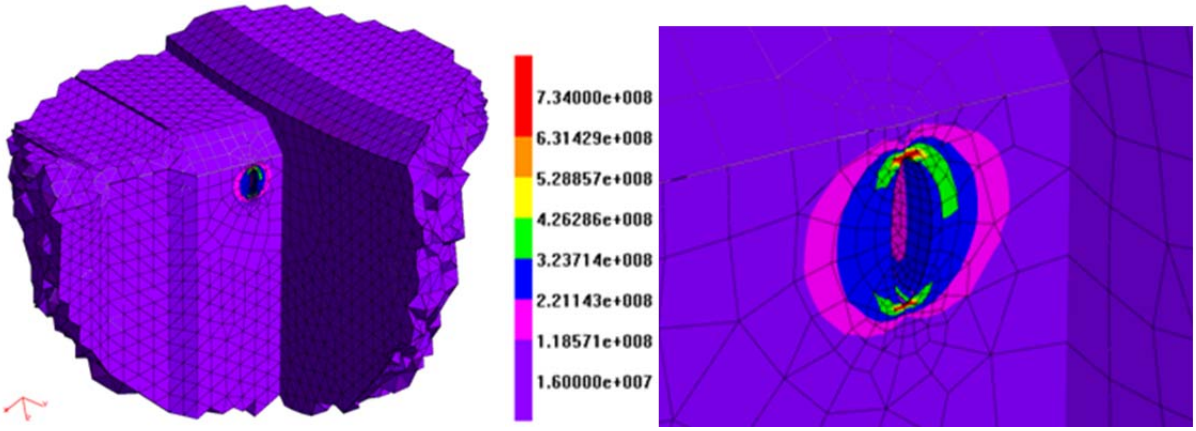

Figure 11. (a) Von Mises stress scenario for LC approach; initial crack configuration and load case N. 3; (b) close up of the von Mises stress scenario in the crack surroundings for LC approach; initial crack configuration and load case N. 3.

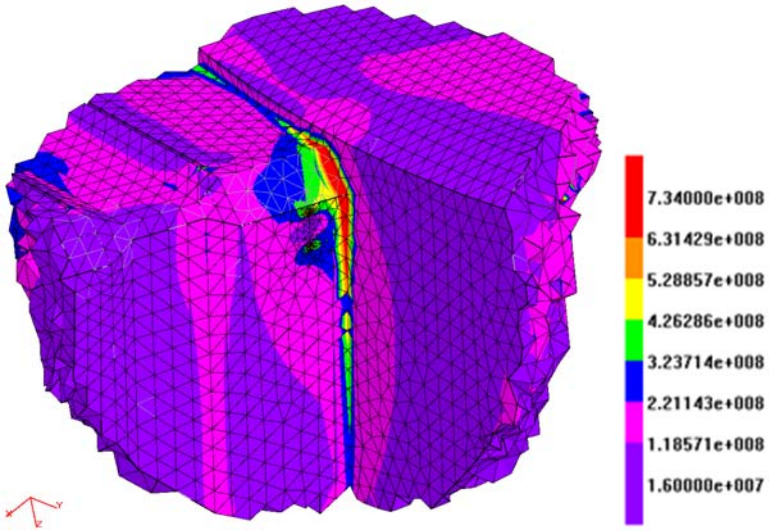

Figure 12. Von Mises stress scenario from FD approach; initial crack configuration and load case N. 3.

SIFs computed by the FD approach [10] are compared with those obtained by FL and LC approaches for the five different loading cases (Fig. 13). Such SIFs for the initial crack configuration show a perfect match, proving the correct implementation of the superposition principle to the LEFM problem considered.

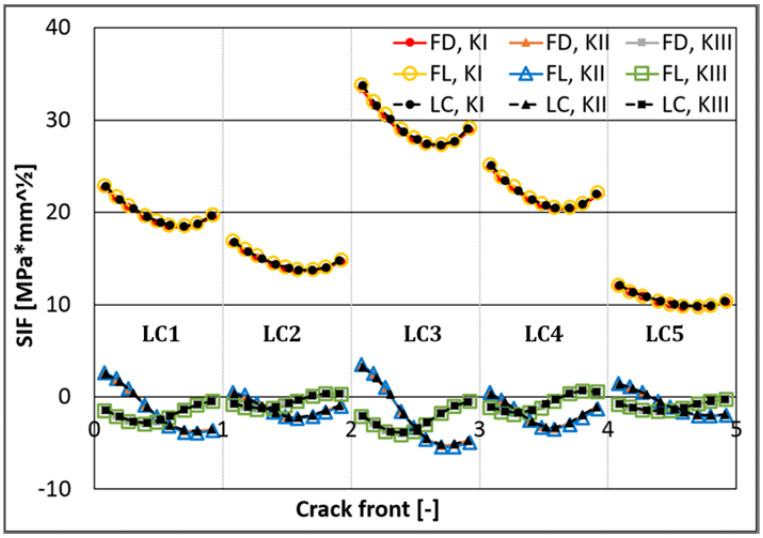

Figure 13. Initial SIF values for the FD, FL, LC approaches; weekly load spectrum.

Once the FEM analyses are completed and the DBEM model is created, a step-by-step crack growth can be predicted, considering each single growth step comprehensive of the following phases:

1. crack insertion;
2. crack faces loading;
3. linear-elastic DBEM analysis and corresponding SIFs evaluation;
4. life prediction;
5. new crack front prediction.

As previously said, the application of traction (FL) or displacement (FD) boundary conditions to the DBEM cut surfaces would represent an approximation due to the continuously increasing crack sizes and the consequent decreasing of the DBEM model stiffness. In addition, such boundary conditions generally come from a FEM global model in which the presence of the crack has not been considered. On the contrary, the proposed approach does not present such approximation, as the traction boundary conditions applied on the crack faces are rigorously computed from the uncracked FEM domain, as theoretically dictated by the superposition principle.

The crack propagation, subdivided in 16 steps, is computed considering an average crack advance per step ranging between 1 and 1.5 mm. The final considered crack shape, with related tractions applied on the crack face elements, is shown in Fig. 14: a slight kinking of the growing crack is visible consistently with the mixed mode conditions (Fig. 13).

Results in terms of crack advances vs. cycles and K_{eff} during growth are reported in Figs. 15-16 respectively: it is possible to observe that the K_{eff} values, even if higher than threshold, turn out to be lower than K_c up to the final considered scenario, which consequently is judged subcritical. Fig. 17 shows the von Mises stresses in the crack surroundings, related to the last considered growth-step computed with the LC approach (load case N° 3): such stresses, as previously said, are not prone to a physical interpretation.

Effective SIF values are computed by using the Yaoming-Mi formula [17]:

$$K_{eff} = \sqrt{(K_I + |K_{III}|)^2 + 2K_{II}^2} \quad (5),$$

and its variation in the cycle provides the ΔK_{eff} to be used in the Paris' or Forman's law (Eqs. 3, 4).

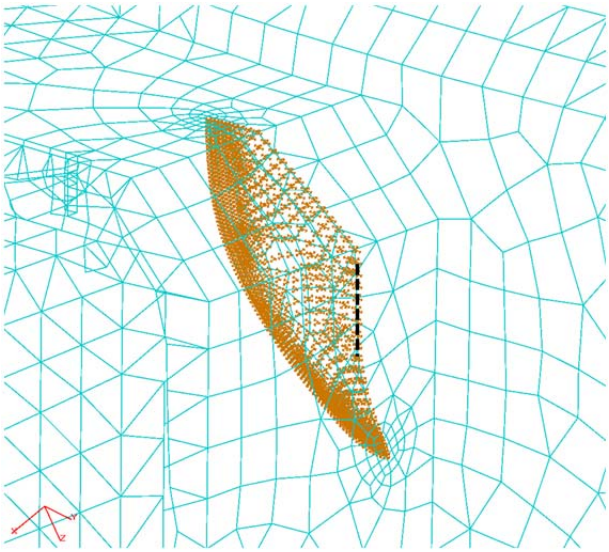

Figure 14. Final crack shape; traction BCs applied on crack face elements in orange; dashed black line representing the initial edge of the inserted crack.

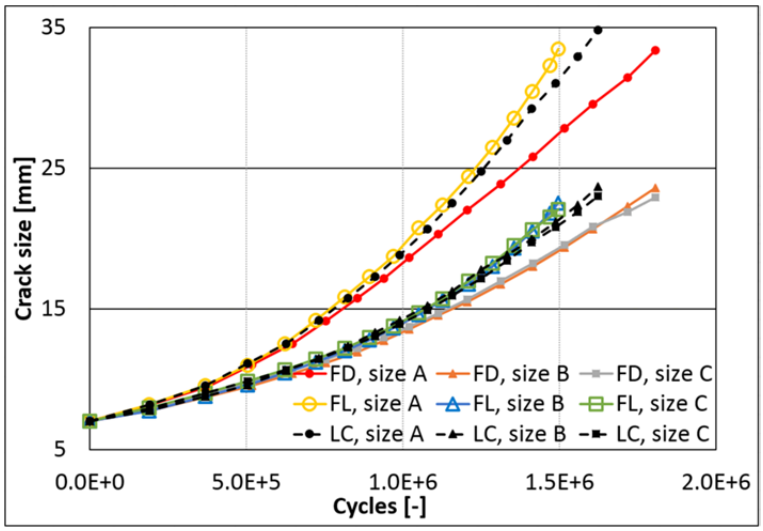

Figure 15. Crack sizes vs. number of cycles under weekly load spectrum.

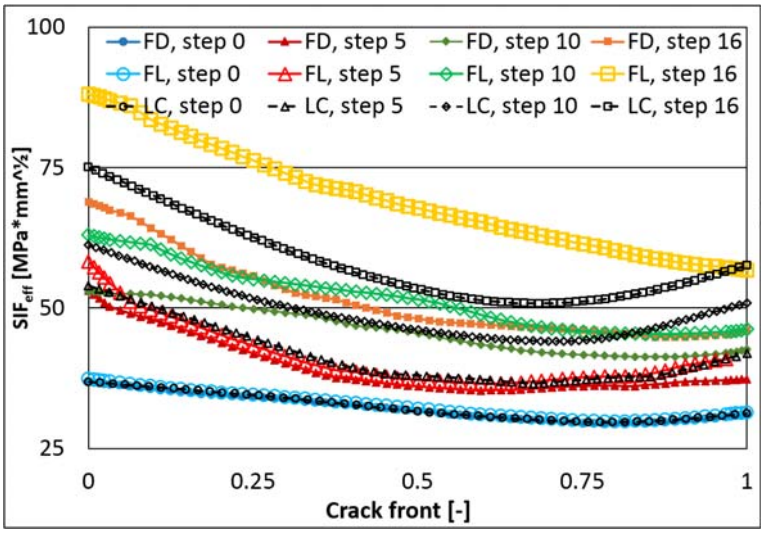

Figure 16. Effective SIF vs. number of cycles under weekly load spectrum.

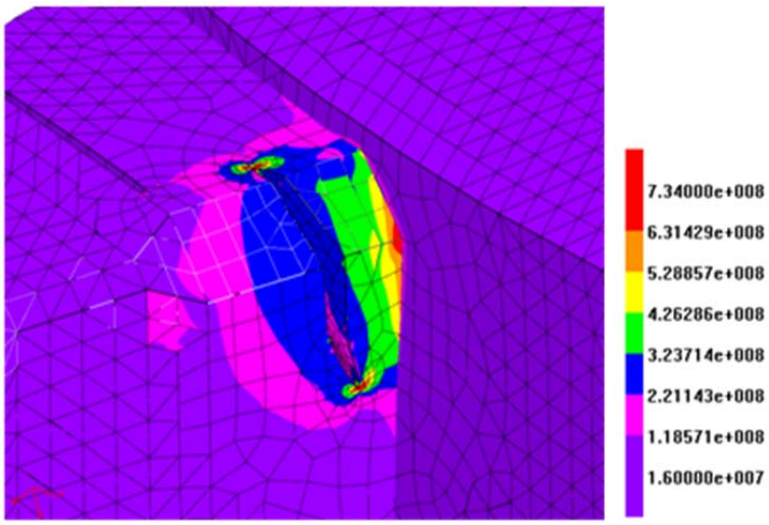

Figure 17. Close up of the von Mises stress scenario in the crack surroundings from LC approach; final crack configuration and load case N. 3.

Daily spectrum

As performed for the weekly spectrum, a second crack-growth simulation has been performed considering the four load cases representative of daily spectrum. Again, it is possible to observe the progressively increasing difference between the three approaches, with results precisely overlapped at step 0 (Fig. 18) and progressively diverging along with crack extension (Fig. 19). Such results in terms of crack advances vs. cycles and K_{eff} during growth are reported in Figs. 19-20 respectively. The crack propagation is again split in 16 propagation steps, with average advances per step equal to 1 mm for the initial steps and 1.5 mm for the last steps.

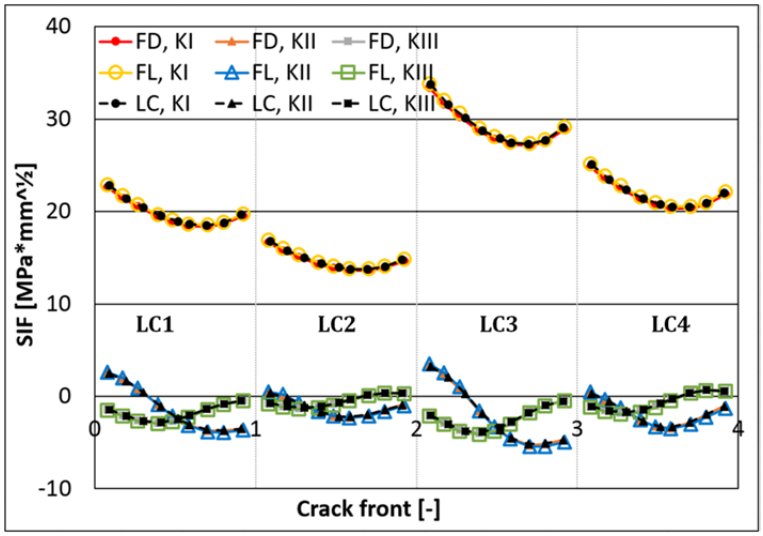

Figure 18. Initial SIF vales for the FD, FL, LC approaches; daily load spectrum.

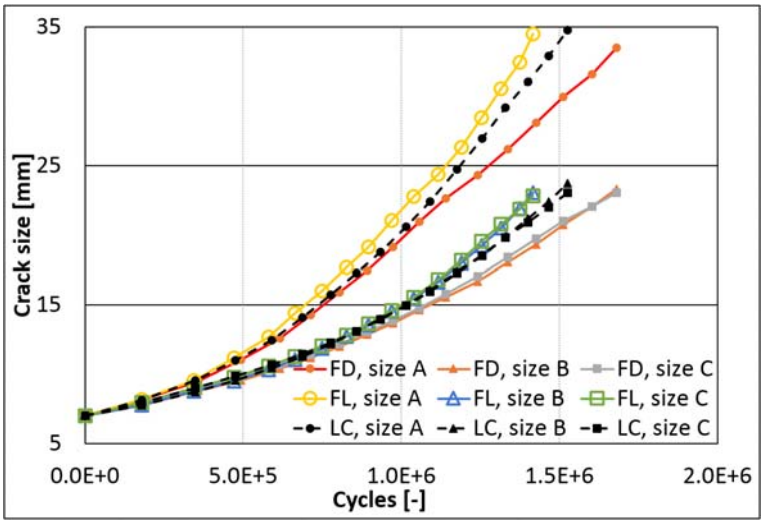

Figure 19. Crack sizes vs. number of cycles; daily load spectrum.

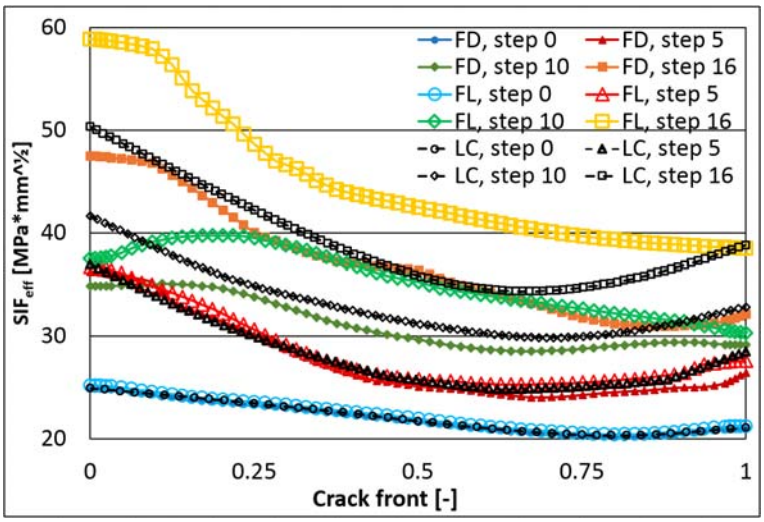

Figure 20. Effective SIF vs. number of cycles; daily load spectrum.

Computational advantages

LC runtimes are strongly reduced, in comparison to LC or FD approaches, due to the smaller DBEM model and to the simpler pure stress analyses required for SIFs assessment. Runtimes (averaged between analyses with daily and weekly load spectra) are listed in Table 6, showing to which extent LC approach is faster than FD/FL approaches.

DBEM analysis	FD/FL	LC	
SIFs at initial step	59	21	-64%
SIFs at final step	151	27	-82%
Whole crack growth	1704	414	-76%

Table 6. Runtimes comparison between FD/FL and LC.

7. Conclusions

Two crack-growth simulations have been performed to analyse the behaviour of the most critical crack, discovered on a W7-X LSE, when undergoing two different load spectra.
The proposed LC approach, in which the DBEM loads consist just of FEM stresses applied on the DBEM crack face elements, allowed to work out the LEFM problem with some advantages over the FD or FL approaches.
Although SIF values along crack front provided by the different FD, FL and LC approaches are perfectly overlapped for the initial crack configuration, differences arise when the crack is growing through the DBEM domain. The reason is twofold: the FD/FL methods do not consider the variability of BCs along with the crack-growth and suffer from an approximation when using a FEM uncracked model to obtain the DBEM boundary conditions. On the contrary, the LC approach, updating step-by-step the BCs with which it computes SIFs, circumvents the approximations above described, predicting CGRs in between the conservative (FL) and non-conservative (FD) approaches.
Several advantages of LC, in terms of accuracy as well as runtimes, against the previously considered approaches with fixed displacement/traction boundary conditions, have been presented and discussed in this paper.
All different approaches reported in previous papers together with the current outcomes, turn out to be highly useful to judge the risk of unstable crack-growths in large structures.

References

[1] Bykov V et al. Structural analysis of W7-X: Overview. *Fusion Engineering & Design*, 2009; 84, 215–219.
[2] Pedersen T S et al. Confirmation of the topology of the Wendelstein 7-X magnetic field to better than 1:100,000. *Nat. Commun.* 2016; 7, 13493 doi: 10.1038/ncomms13493.

[3] Klinger T et al. Performance and properties of the first plasmas of Wendelstein 7-X. *Plasma Phys. Control.* Fusion 2017; 59, 014018 (8pp).
[4] EN ISO 23277, CEN, Brussels, 2010.
[5] Corato V et al. Detailed design of the large-bore 8T superconducting magnet for the NAFASSY test facility. Supercond. Sci. Technol. 2015; 28:1–9.
[6] Citarella R, Cricrì G, Lepore M, Perrella M. DBEM and FEM Analysis of an Extrusion Press Fatigue Failure. *Advanced Structured Materials* 2010; 3:181-191.
[7] Citarella R. MSD Crack propagation on a repaired aeronautic panel by DBEM. *Advances in Engineering Softwar*e 2011; 42 (10), 887-901.
[8] Citarella R, Carlone P, Sepe R, Lepore M. DBEM crack propagation in friction stir welded aluminum joints. *Advances in Engineering Software* 2016; 101:50-59.
[9] Citarella R, Lepore M, Shlyannikov V, Yarullin R. Fatigue surface crack growth in cylindrical specimen under combined loading. *Engineering Fracture Mechanics* 2014; 131:439–453.
[10] Citarella R et al. Coupled FEM-DBEM method to assess crack growth in magnet system of Wendelstein 7-X. *Frattura ed Integrità Strutturale* 2013; 26:92-103.
[11] Citarella R, Carlone P, Lepore M, Sepe R. Hybrid technique to assess the fatigue performance of multiple cracked FSW joints. *Engineering Fracture Mechanics* 2016; 162:38-50.
[12] Citarella R, Cricrì G, Lepore M, Perrella M. Thermo-Mechanical Crack Propagation in Aircraft Engine Vane by Coupled FEM-DBEM Approach. *Advances in Engineering Software* 2014; 67,:57-69.
[13] Citarella R, Giannella V, Vivo E, Mazzeo M. FEM-DBEM approach for crack propagation in a low pressure aeroengine turbine vane segment. *Theor Appl Fract Mec* 2016; 86:143-152.
[14] Citarella R, Lepore M, Perrella M, Fellinger J. Coupled FEM-DBEM approach on multiple crack growth in cryogenic magnet system of nuclear fusion experiment 'Wendelstein 7-X'. *Fatigue Fract. Eng. Mater. Struct*. 2016; 39:1488-1502.
[15] Wilson WK, YU I-W. The use of J-integral in thermal stress crack problems. *Int J Fract* 1979; 15:377-387.
[16] Dassault Systèmes Simulia Corp. Abaqus Analysis User's Manual, Version 6.12.1, Providence, RI, USA, 2011.
[17] BEASY. BEASY V10r14 Documentation C.M. BEASY Ltd, 2011.
[18] Sih GC, Cha BCK. A fracture criterion for three-dimensional crack problems. *J Engng Fract Mech* 1974; 6:699–732.
[19] Rigby RH, Aliabadi MH. Mixed-mode J-integral method for analysis of 3D fracture problems using BEM. *Engng Anal Boundary Elem* 1993; 11:239–56.
[20] Rigby RH, Aliabadi MH. Decomposition of the mixed-mode J-integral – revisited. *Int J Solids Struct* 1998; 35, 17:2073–99.
[21] Paris P, Gomez M, Anderson W. A rational analytic theory of fatigue. *Trends Eng.* 1961; 13:9–14.
[22] Forman RG, Kearney VE, Engle RM. Numerical analysis of crack propagation in cyclic-loaded structures. *J. of Basic Engineering* Trans. ASME, 1967; 89:459- 464.